

About the Influence of Wind Tunnel Walls, Tower and Nozzle on the Performance of a Model Wind Turbine

Annette Klein (née Fischer), Sven Zabel, Thorsten Lutz, and Ewald Krämer

Abstract The influence of wind tunnel walls, tower and nozzle on the performance of a model wind turbine is investigated in the present paper using Computational Fluid Dynamics (CFD). The model wind turbine has a radius of 1.5 m and is located in a wind tunnel with a cross section of 4.2 m × 4.2 m. Global loads, angle of attack distributions as well as flow fields are compared to each other to evaluate the influence of the different configurations.

1 Introduction

In order to increase the competitiveness of wind energy against conventional sources of energy, wind turbines have to be improved and further developed. However, in an early state of development, new applications can't be tested on real wind turbines but have to be investigated on model wind turbines. Such experiments are cheaper than experiments on real wind turbines and in addition, the same inflow conditions can be repeated in a wind tunnel as often as necessary. Cheaper and faster than experiments on turbines are CFD (computational fluid dynamics) simulations of wind turbines. Thereby, the same inflow conditions can be repeated as well, but moreover, numerical models of full size turbines can be simulated and the inflow conditions can be changed easier than in a wind tunnel.

In advance of such simulations, the suitability of the CFD model to display the loads on and the flow around wind turbines has to be validated by experiments. Therefore, simulations of the experimental setup are necessary. As not all components, which are present in the wind tunnel (probe rigs, bottom plate, steps, etc.), can be considered in the simulation and in order to save computational time, the numerical setups are often simplified. As wind turbine rotors are rotationally symmetric, it can be sufficient to simulate only one blade and use rotationally periodic boundary conditions. Thereby, the tower has to be neglected. If the blockage ratio of a wind

A. Klein (née Fischer) • S. Zabel • T. Lutz (✉) • E. Krämer
Institute of Aerodynamics and Gas Dynamics (IAG), University of Stuttgart, Pfaffenwaldring 21,
70569 Stuttgart, Germany
e-mail: fischer@iag.uni-stuttgart.de; lutz@iag.uni-stuttgart.de

tunnel, which is defined as the rotor swept area divided by the wind tunnel cross section area, is smaller than 10%, no wind tunnel effects should be experienced, according to Schümann [22]. In such a case, the wind tunnel walls could be neglected, too. However, for each experimental setup it should be checked, which components can be neglected in the simulation, in order to get a good accordance between simulation and experiment with as little computational time as possible.

There are several publications about the simulation of model wind turbines. In the *MEXICO* project [19], as well as in the *INNWIND.EU* project [11], model wind turbines in an open jet section are investigated experimentally and numerically. The *NREL PHASE-VI* model wind turbine was investigated, amongst other, by Sørensen et al. [23] numerically. The closed test section in this investigation had a blockage ratio of 8.8% and only small blockage effects occur. Krogstad and Lund [13] expected also only small blockage effects in their experimental and numerical investigation of a model wind turbine in a wind tunnel with a blockage ratio of 11.8%. Schümann [22], however, experienced an effect of the wind tunnel walls for his investigations of a model wind turbine with 14% blockage ratio.

The model wind turbine, which will be investigated in the present paper, is the Berlin Research Turbine (*BeRT*), which was designed and built by the Technical University of Berlin in cooperation with the *SMART BLADE GmbH*. It is investigated in the course of the *DFG PAK 780* project [16], where six partners from five different Universities (TU Berlin, University of Stuttgart, RWTH Aachen, Technical University of Darmstadt and Carl von Ossietzky University Oldenburg) are working together on the field of wind turbine load control under realistic turbulent inflow conditions. Thereby, different load alleviation systems are investigated numerically and experimentally, amongst other, on the *BeRT* turbine.

A one third model of the *BeRT* turbine was already simulated under uniform free stream condition with a large-eddy (LES) approach [6]. As the turbine is located in the closed 4.2 m × 4.2 m test section of the great wind tunnel (*GroWiKa*) of the TU Berlin, where a blockage ratio of over 40% is achieved, the wind tunnel walls must not be neglected in the simulations. In order to estimate the influence of the wind tunnel environment, Reynolds-averaged Navier-Stokes simulations (*RANS*) under uniform free stream condition, but also with a wind tunnel with a slightly higher blockage ratio than in the *GroWiKa*, were performed by Fischer et al. [3] and the results were compared to each other. This approximated wind tunnel had a blockage ratio of around 50%, was realized on the one hand with a slip wall and on the other hand with a no-slip wall and had, due to the one third model of the turbine, a cylindrical cross section instead of an angular one. The minimal distance between the blade tip and the wind tunnel wall was the same as in reality. As expected for such a high blockage ratio, the wind tunnel walls had a huge influence on the performance of the wind turbine, which did not behave like a free stream turbine any more, as even the Betz limit [5] was exceeded. In the present investigation, the influence of wind tunnel walls, tower and a nozzle, which is located 2.5R downstream the turbine, on the loads, the angle of attack (AoA) distribution and on the flow field is investigated and compared to each other in order to estimate which simplifications in the numerical setup are acceptable.

2 Model Wind Turbine

The *BeRT* turbine has a radius of $R = 1.5$ m and a hub height of $h = 2.1$ m. In the present investigations, the inflow velocity is set to $v_{inflow} = 6.5$ m/s and the turbine rotates with 180 rpm. This leads to a tip speed ratio of $\lambda = 4.35$. The blades of the turbine consist of only one cross section, which is based on the *CLARK-Y*-airfoil, and are exchangeable. The choice fell on this airfoil as it can provide attached flow for low Reynolds numbers and it has a good effectiveness with leading and trailing edge flaps. Those flaps can be used for active and passive load alleviation, which is investigated on this turbine in the course of the *DFG PAK 780* project [16]. More information about this turbine can be found in Pechlivanoglou et al. [17]. The turbine is placed in the settling chamber of the *GroWiKa* of the TU Berlin, which was converted to a 4.2 m \times 4.2 m test section. As a consequence, the nozzle, which is usually placed in front of a test section, is now located behind the turbine.

3 Numerical and Computational Details

3.1 Numerical Methods

The *RANS* simulations of the *BeRT* turbine are performed using the block structured code *FLOWer*, which was developed by the *German Aerospace Centre* (DLR) in the course of the *MEGAFLOW* project [14]. It uses the finite volume method to solve the unsteady Reynold-averaged Navier-Stokes equations (*URANS*) on block-structured grids. For the spatial discretisation, a second order central discretisation scheme *JST* [8] is used and the time is discretised with an implicit dual time stepping scheme [7]. Several state of the art turbulence models are implemented, but for the present case, the *Menter SST* turbulence model was used. All components are meshed separately with a fully resolved boundary layer, ensuring $y^+ \approx 1$ of the first cell, and are overlapped using the *CHIMERA* technique [1]. For the numerical simulation of wind turbines, a process chain, which was developed at the Institute of Aerodynamics and Gas Dynamics (*IAG*) [15], and which was also used in several other wind energy projects [20, 21, 24], was used for the present investigations, too.

3.2 Performance of the Solver

For the present investigations, a *FLOWer* version from 2016 was used, which had only minor changes concerning the performance of the version compared to the version which was used for the investigations in [4]. Therefore, the strong and weak scaling test, as shown in [4], was over taken for the present paper (Fig. 1).

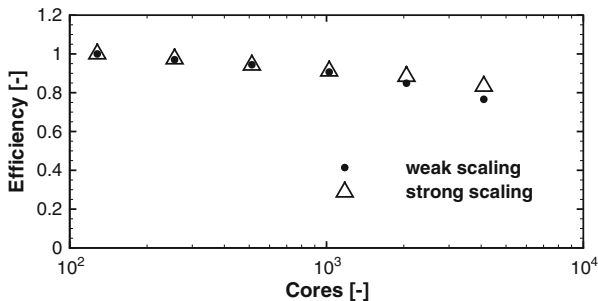


Fig. 1 Efficiency of *FLOWer* on *Cray XC40* using *ifort* fortran compiler and a constant cell loading of 32^3 for each MPI process in case of weak scaling and 4096 times 32^3 cells in case of strong scaling. Taken from [4]

Table 1 Characteristics of the *BeRT* turbine and the wind tunnel

Rotor radius (m)	1.5
Tower height (m)	2.1
Cone angle (°)	0
RPM (-)	180
Inflow velocity (m/s)	6.5
Wind tunnel cross section (m × m)	4.2 × 4.2

For up to 1024 cores, the weak and strong scaling showed the same efficiency. For more cores, the efficiency of the strong scaling is slightly better than for the weak scaling. With a total usage of 4096 cores, *FLOWer* has an efficiency of 0.77 for the weak scaling and of 0.83 for the strong scaling. As an example for an average simulation, the case of the full wind turbine without tower in the far field is presented. The total amount of approximately 36 million cells was computed on 1296 cpus. A simulation of 73 revolutions with 120 to 240 time steps per revolution and 30 inner iterations, as shown in the present investigations, consumes approximately 140 h (wall clock time) and consequently 181,000 cpuh.

3.3 Numerical Setup

Table 1 gives an overview of the turbine and its operating condition used for the investigations in this paper.

Four different cases are investigated in the present paper. One case is simulated under far field condition (hereinafter designated as *FF*), two cases include wind tunnel walls with constant cross section (hereinafter designated as *WT1*) and another case with wind tunnel walls and a nozzle $2.5R$ behind the rotor plane is designated as *WT2*. Simulations of the pure rotor are denominated with the affix *rot*, if the tower is included, the affix is *tow*. The numerical setup of the model wind turbine consists of nine (*rot*) respectively eleven (*tow*) independent meshes which are overlapped using

Table 2 Characteristics of the different setups

	FF_{rot}	$WT1_{rot}$	$WT1_{tow}$	$WT2_{tow}$
Cell number	35,992,576	31,678,976	33,529,856	34,884,608
No. of grids	9	9	11	11
Background	FF	WT	WT	WT
Tower	–	–	x	x
Nozzle	–	–	–	x

the *CHIMERA* technique [1]. Table 2 gives an overview of the different setups used for the investigations in this paper.

The blade mesh is of CH-topology and was created through a script, which was developed at the *IAG*. It has a fully resolved boundary layer (37 cell layers), ensuring $y^+ < 1$ for the first grid layer. In radial direction, 101 cells are used, around the airfoil 181, leading to an amount of approximately 5.5 million cells per blade. The mesh for the blade connection, hub, nacelle, tower connection and tower are created manually. The background grid for the far field case was generated with an automated script [12] and hanging grid nodes are used for the refinement. Thereby, refinements can be realised only where it is needed, whereas usual refinement in a H-topology is leading to refinements at unnecessary spots. The grid is approximately $20.5R$ long ($8R$ upstream and $12.5R$ downstream of the rotor plane), approximately $24.6R$ wide and has a height of approximately $14R$. According to Sayed [18], this extension is big enough to prevent any influence of the boundary conditions on the turbine. The bottom is a slip wall, all other boundaries are realised as far field. The cells around the turbine are $0.025\text{ m} \times 0.025\text{ m} \times 0.025\text{ m}$ and at the outflow $0.1\text{ m} \times 0.1\text{ m} \times 0.1\text{ m}$. The far field mesh has an overall amount of 13.7 million cells. In the experiment, the *BeRT* turbine is located in the settling chamber of the *GroWiKa* and the rotor plane is located 1.245 m behind the beginning of the chamber. This chamber has a cross section of $4.2\text{ m} \times 4.2\text{ m}$ and is 5 m long. However, in order to prevent disturbances of the boundary condition to convect to the turbine, the wind tunnel was extended in the numerical setup. It is approximately $16.5R$ long, whereby the rotor plane is located approximately $7.5R$ downstream of the inflow boundary condition and thus far away enough according to Sayed [18]. Like for the far field case, the cells around the turbine measure $0.025\text{ m} \times 0.025\text{ m} \times 0.025\text{ m}$. At the inflow boundary, the cells have a size of $0.4\text{ m} \times 0.025\text{ m} \times 0.025\text{ m}$ and at the outflow of $0.2\text{ m} \times 0.025\text{ m} \times 0.025\text{ m}$. As no hanging grid nodes were used here, only a coarsening in streamwise direction was possible. The wind tunnel walls are realized as slip walls, whereby a calculated displacement thickness is added on the real walls, leading to a continuous reduction of the cross section for the settling chamber. In front and behind the chamber, the cross section is constant. For the setup *WT2*, a nozzle with a total length of 3.0 m and a tapering of 2.2 follows the settling chamber. The inflow boundary is realized as far field and for *WT1*, the outflow boundary, too. For *WT2*, the outflow boundary had to be changed to constant pressure in order to maintain mass continuity. An

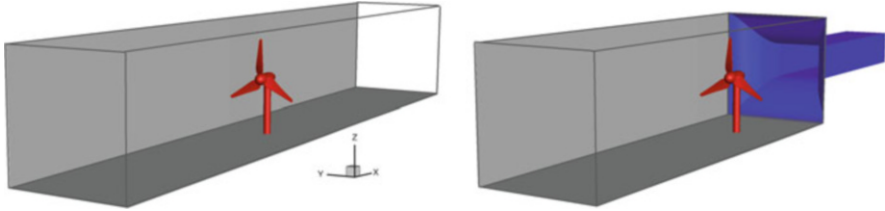


Fig. 2 Setup for $WT1_{low}$ (left) and $WT2_{low}$ (right)

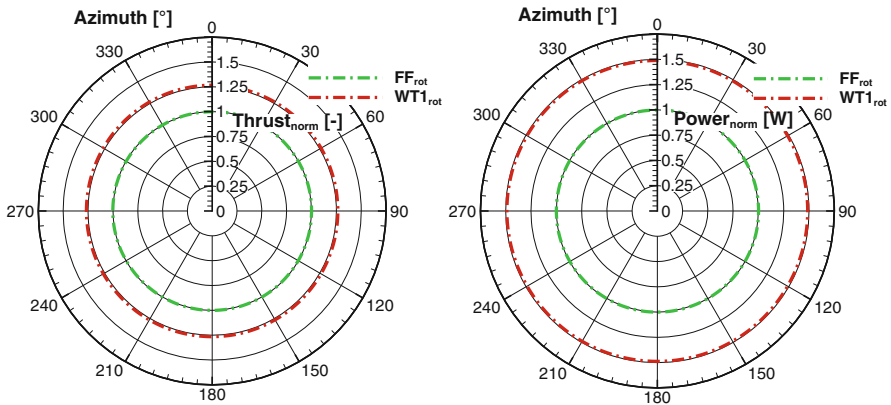


Fig. 3 Thrust (left) and power (right) over one revolution for FF_{rot} and $WT1_{rot}$, normalised with the averaged value of FF_{rot} . Azimuth indicates the position of the first blade

investigation of the grid convergence index according to Celik [2] was already performed for a one third model by Fischer et al. [3] and the grids for the full turbine were created according to the results of this study. Figure 2 shows the setup for $WT1_{low}$ and $WT2_{low}$.

4 Results

4.1 Influence of the Wind Tunnel Walls

As already reported by Fischer et al. [3], the wind tunnel walls have a large influence on the flow around the turbine. Figure 3 shows the normalized thrust and power of the whole turbine for FF_{rot} and $WT1_{rot}$. The azimuth indicates the position of the first blade, whereby an azimuth of 0° means, that the blade is pointing upward.

Due to the presence of the wind tunnel environment, thrust is increased by approximately 25%, power is increased by even 50%. This is in good accordance to the results from Fischer et al. [3] who found an increase by 25–30% respectively

67–78% at an inflow velocity of $v_{inflow} = 8$ m/s and a blockage ratio of approximately 50%. This increase is due to the limited space caused by the wind tunnel walls. The wind turbine doesn't work like a free stream turbine any more as the wake can not expand like under far field condition, leading to higher velocities in the rotor plane and consequently to higher loads. More information about this topic can be found in Fischer et al. [3].

4.2 Influence of the Tower

As the wind tunnel walls have a large impact on the performance of the turbine, the walls will be considered in the following subsections. Figure 4 shows the normalized thrust and power of the whole turbine for $WT1_{rot}$ and $WT1_{tow}$.

Whereby thrust and power of the pure rotor are almost constant over one revolution, the curve for the setup including tower shows higher variations caused by the displacement effect of the tower. There are three drops in thrust and power at 60°, 180° and 300° azimuth with a phase shift of 120°, which is characteristic for a three bladed turbine. Moreover, three maxima at approximately 0°, 120° and 240° are visible.

Table 3 shows the mean values and the amplitude for thrust and power for one revolution.

It can be seen, that the tower shadow results in fluctuations as the lower velocity in front of the tower, due to the blockage effect, leads to a short-term load reduction. However, for the case under investigation, the influence of the tower does not only lead to a decrease of the load in front of the tower, but also to a higher maximum. This is due to the fact of the limited space around the turbine. In the wind tunnel, the tower increases the blockage even more, leading to higher velocities around the

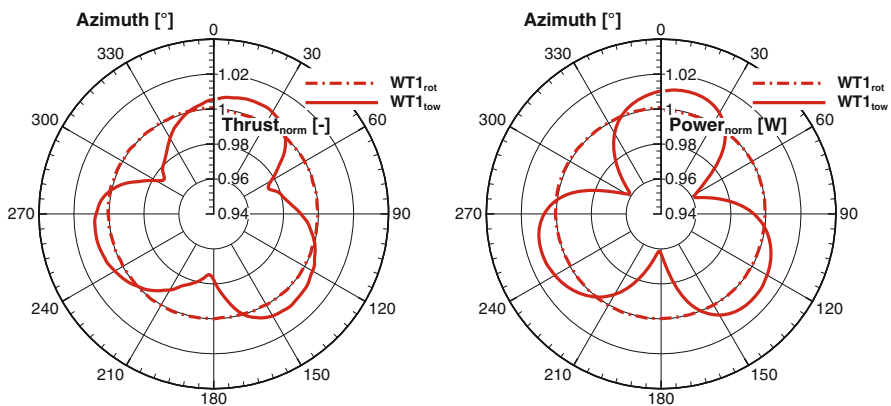


Fig. 4 Thrust (left) and power (right) over one revolution for $WT1_{rot}$ and $WT1_{tow}$, normalised with the averaged value of $WT1_{rot}$. Azimuth indicates the position of the first blade

Table 3 Thrust and power over one revolution, Δ value with regard to the mean value of $WT1_{rot}$

	Thrust (N)		Power (W)	
	$WT1_{rot}$	$WT1_{tow}$	$WT1_{rot}$	$WT1_{tow}$
Mean value	163.1	162.4	730.1	725.7
Δ Mean	–	–0.43%	–	–0.60%
Amplitude	–	2.8	–	18.3

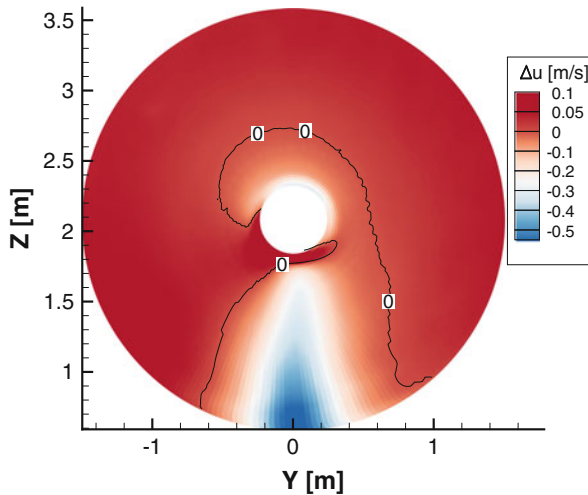


Fig. 5 Difference in streamwise velocity (averaged over one revolution) between $WT1_{tow}$ and $WT1_{rot}$ ($\Delta u = u_{WT1_{tow}} - u_{WT1_{rot}}$) in the rotor plane, viewing direction is upstream

turbine compared to the case $WT1_{rot}$. This can be seen in Fig. 5, where the difference of the averaged velocity between $WT1_{tow}$ and $WT1_{rot}$ in the rotor plane is plotted. Except in front of the tower, the velocity is higher for the case including tower. If a blade is in front of the tower, it is in the area of lower velocity. If no blade is in front of the tower, all blades are consequently in areas of higher velocity compared to the case without tower. These differences lead to the higher maxima. As the loads are not only decreased in front of the tower but also increased next to the tower, the minima and maxima partly offset one another, leading only to a small change of the mean value.

Even though the velocity around the tower and in the rotor plane is higher, the area in front of the tower has such an influence, that the averaged AoA is reduced throughout the majority of the blade radius, compared to the case without tower (see Fig. 6), consequently reducing the mean values of thrust and power. Information about the determination of the AoA distribution can be found in [10] and [9].

Another aspect is, that the influence of the tower is more pronounced in power than in thrust for both, mean value and amplitude. As the lift of an airfoil is at least one order higher than drag, the resulting force is more oriented towards lift and therefore to the normal of the rotor plane. And as power originates from the driving

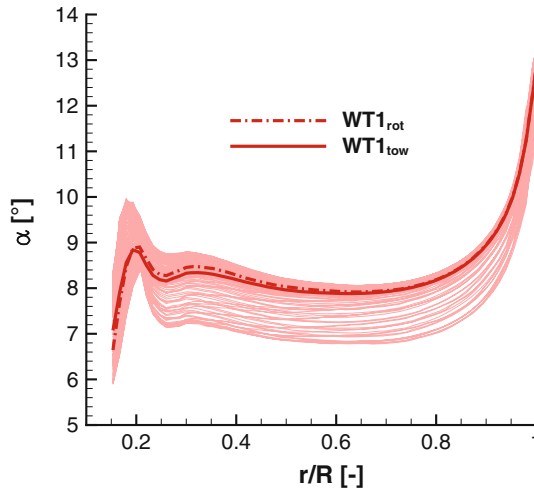


Fig. 6 Angle of attack distribution over the blade, averaged over one revolution. Light curves show the solutions of $WT1_{tow}$ every 1.5° azimuth

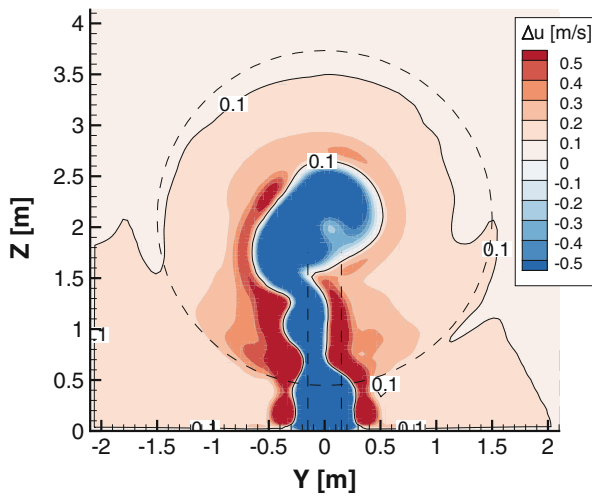


Fig. 7 Difference in streamwise velocity between $WT1_{tow}$ and $WT1_{rot}$, averaged over one revolution ($\Delta u = u_{WT1_{tow}} - u_{WT1_{rot}}$). $1R$ downstream the rotor, viewing direction is upstream

force, which lies in the rotor plane, it is more sensitive to AoA variations than thrust, which originates from the force perpendicular to the rotor plane.

Figure 7 shows the velocity difference between $WT1_{tow}$ and $WT1_{rot}$ $1R$ behind the rotor for the complete wind tunnel cross section. In addition, the rotor and the tower are indicated by dashed lines.

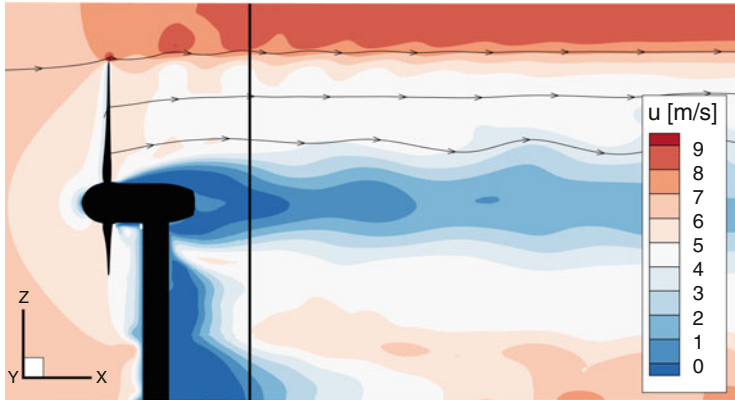


Fig. 8 Snapshot of the streamwise velocity for $WT1_{tow}$ in the middle of the wind tunnel ($y = 0m$) including three streamtraces. Wind turbine illustrated in black, black line indicates the position of Fig. 7

The velocity in the wake of the turbine is higher for the case with tower, indicated by the red colours dominating the plot outside of the tower blockage. Left and right of the tower, due to the blockage, the velocity is even higher. A cut through the flow field of the wind tunnel at $y = 0m$ is shown in Fig. 8.

It is a snapshot and the turbine is illustrated in black. The vertical black line is positioned at $x = 1.5m$, which corresponds to the evaluation position of Fig. 7. In addition, three streamtraces are shown. These lines are almost horizontal, indicating the only slight expansion of the wake. The wake space of the nacelle, as well as of the tower, can be seen, too. Moreover, the speed-up in the bypassing flow, as already described by Fischer et al. [3], is clearly visible.

4.3 Influence of the Nozzle

As the influence of the tower on the loads is quite strong, it is considered in the following by comparing case $WT1_{tow}$ and $WT2_{tow}$. Figure 9 shows the normalized thrust and power of the whole turbine for these two cases.

Due to the nozzle, the mean values of thrust and power are increased.

Table 4 shows the mean values and the amplitude for thrust and power for one revolution for $WT1_{tow}$ and $WT2_{tow}$ with regard to $WT1_{tow}$ in order to estimate the influence of the nozzle.

As already seen in the load distribution, the mean values are increased due to the nozzle. And again, the influence on the mean value is more pronounced for power than for thrust. The amplitudes, however, are stronger in the case without nozzle. In Fig. 10, the velocity difference between $WT2_{tow}$ and $WT1_{tow}$ are plotted in the rotor plane.

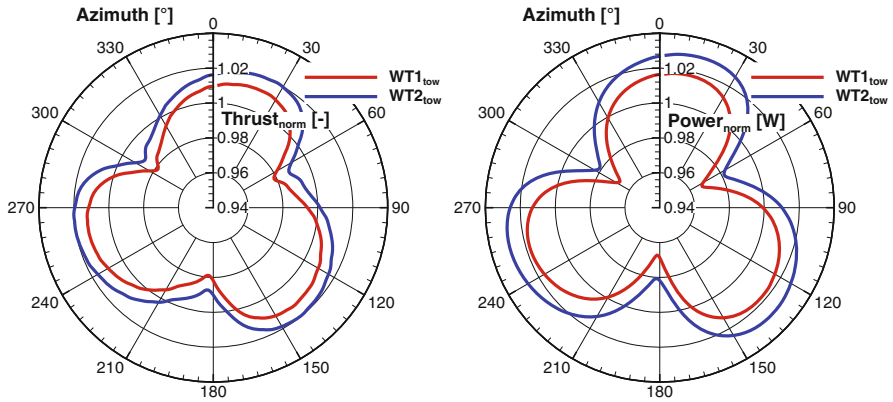


Fig. 9 Thrust (left) and power (right) over one revolution for $WT1_{tow}$ and $WT2_{tow}$, normalised with the averaged value of $WT1_{tow}$. Azimuth indicates the position of the first blade

Table 4 Thrust and power over one revolution, Δ values with regard to the corresponding values of $WT1_{tow}$

	Thrust (N)		Power (W)	
	$WT1_{tow}$	$WT2_{tow}$	$WT1_{tow}$	$WT2_{tow}$
Mean value	162.4	163.7	725.7	734.6
Δ Mean	—	0.80%	—	1.23%
Amplitude	2.8	2.6	18.3	17.3
Δ Amplitude	—	-7.14%	—	-5.46%

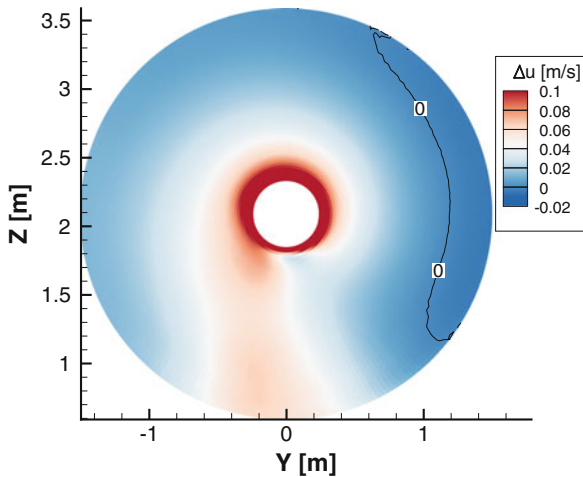
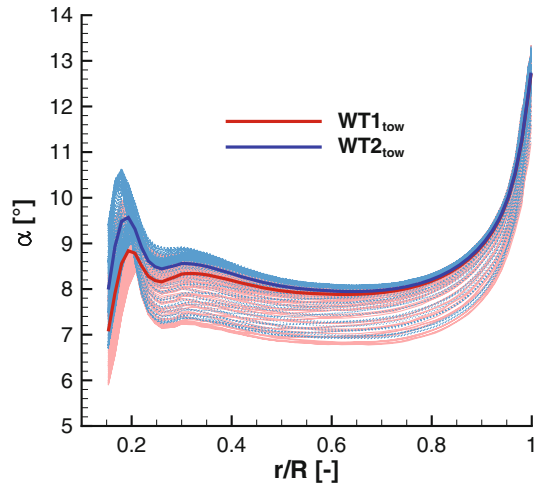


Fig. 10 Difference in streamwise velocity (averaged over one revolution) between $WT2_{tow}$ and $WT1_{tow}$ ($\Delta u = u_{WT2_{tow}} - u_{WT1_{tow}}$) in the rotor plane, viewing direction is upstream

Fig. 11 Angle of attack distribution over the blade, averaged over one revolution. Light curves show the solutions for every 1.5° azimuth



It can be seen that, especially in the inner part, the velocity is higher for the $WT2_{tow}$ case. Consequently, the level of the AoA distribution is higher, too, which can be seen in Fig. 11. The averaged AoA distribution over one revolution shows, due to the smaller impact of the tower, higher values for the $WT2_{tow}$ case, leading to higher mean values of thrust and power, which was already seen in Table 4. The biggest difference between the AoA distributions can be seen again in the inner part of the rotor.

In Fig. 12, the velocity difference between $WT2_{tow}$ and $WT1_{tow}$ is plotted $1R$ behind the rotor. Again, the rotor and the tower are indicated by dashed lines. It can be seen, that for the wind tunnel with nozzle, the velocity in the outer part of the rotor is slightly increased, whereas it is decreased in the corner of the wind tunnel and around the half radius position. In the inner part of the rotor, however, the velocity is higher compared to the case without nozzle. The tower blockage is less pronounced, as indicated by the higher velocity in the area behind the tower.

Figure 13 shows a snapshot of the streamwise velocity in the middle of the wind tunnel ($y = 0$ m).

The increase of speed in the nozzle is clearly visible. Consequently, the wake is less elongated and even less expanded than in the case without nozzle. The higher velocities in the inner part of the rotor, as already seen in Figs. 10 and 12, might be a result of the deflection of the wake to the middle of the wind tunnel as the tip vortices are sucked into the nozzle. Due to this deflection, the induction of the wake changes, which has in turn, due to Biot-Savart, an influence on the induced velocity in the rotor plane. Moreover, the upstream influence of the nozzle might lead to an acceleration in the middle of the wind tunnel, too. A comparison of the stream traces between Figs. 8 and 13 shows, that due to the nozzle, the stream traces are curved, following the shape of the nozzle as they are sucked in.

In order to differentiate between the influence of the tower and the influence of the nozzle, Table 5 shows the mean values and the amplitude for thrust and power for one revolution for $WT1_{rot}$ and $WT2_{tow}$ with regard to $WT1_{rot}$.

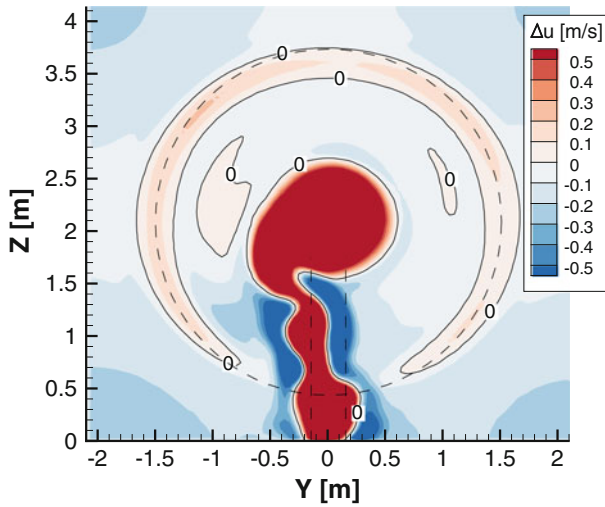


Fig. 12 Difference in streamwise velocity between $WT2_{tow}$ and $WT1_{tow}$, averaged over one revolution ($\Delta u = u_{WT2_{tow}} - u_{WT1_{tow}}$). 1R downstream of the rotor, viewing direction is upstream

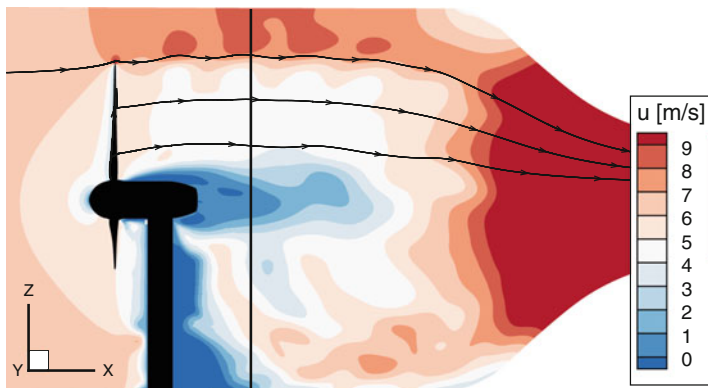


Fig. 13 Snapshot of the streamwise velocity for $WT2_{tow}$ in the middle of the wind tunnel ($y = 0$ m) including three streamtraces. Wind turbine illustrated in black, black line indicates the position of Fig. 12

Table 5 Thrust and power over one revolution, Δ values with regard to the mean value of $WT1_{rot}$

	Thrust (N)		Power (W)	
	$WT1_{rot}$	$WT2_{tow}$	$WT1_{rot}$	$WT2_{tow}$
Mean value	163.1	163.7	730.1	734.6
Δ Mean	—	0.37%	—	0.62%
Amplitude	—	2.6	—	17.3

A comparison of Tables 5 and 3 shows, that the nozzle partly compensates the reduction of the mean values and reduces the amplitudes caused by the tower, as the Δ Mean in Table 5 is bigger and the amplitudes are smaller compared to Table 3.

5 Conclusion

The present article shows numerical investigations of an experimental setup of a model wind turbine including different components, performed with the CFD solver *FLOWer*. The influence of wind tunnel walls, tower and a nozzle downstream of the rotor are investigated and compared. Global loads, velocities and angle of attack distributions as well as flow fields are taken into account. The turbine under investigation is the *BeRT* turbine which has a radius of $R = 1.5$ m, a hub height of $h = 2.1$ m and which is located in the settling chamber of the *GroWiKa* of the Technical University of Berlin.

It turned out, that due to the wind tunnel environment, thrust is increased by approximately 25% and power by 50% for the same inflow velocity and pitch. This strong influence was expected, as the blockage ratio is higher than 40%. Compared to the influence of the walls, the impact of tower and nozzle on the mean values are small (approximately 1%). However, the tower leads to an increase of fluctuations as the blades pass through areas with lower velocity upstream of the tower and areas with higher velocities next to the tower. These load variations should not be neglected in the simulation. The reduction of the mean values of thrust and power, which are also a result of the tower, is partly compensated by the nozzle, which also reduces the amplitudes. This leads to the conclusion that if the tower is taken into account, the nozzle should be considered, too.

To sum up, for such a high blockage ratio, a direct transfer from the wind tunnel results to far field condition is not reasonable. A comparison to the numerical solutions, however, is feasible, but the modelling of the wind tunnel walls, the tower and the nozzle is thereby mandatory.

Acknowledgements The authors gratefully acknowledge the *High Performance Computing Center Stuttgart* for providing computational resources within the project *WEALoads* and the TU Berlin for the provision of the geometric data of the *BeRT* turbine. The studies presented in this article have been funded by the *German Research Foundation* (DFG).

References

1. J.A. Benek, J.L. Steger, F.C. Dougherty, P.G. Buning, *Chimera. A Grid-Embedding Technique* (Arnold Engineering Development Center Arnold Air Force Station, Tennessee Air Force Systems Command United States Air Force, 1986)
2. I.B. Celik, U. Ghia, P.J. Roache et al., Procedure for estimation and reporting of uncertainty due to discretization in {CFD} applications. *J. Fluids Eng.-Trans. ASME* **130**(7), 078001-078004 (2008)

3. A. Fischer, A. Flamm, E. Jost, T. Lutz, E. Krämer, Numerical investigation of a model wind turbine, in *Contributions to the 21st STAB Symposium Braunschweig, Germany 2016*. Notes on Numerical Fluid Mechanics and Multidisciplinary Design. STAB (Springer, Berlin, 2016)
4. A. Fischer, L. Klein, T. Lutz, E. Krämer, Simulations of unsteady aerodynamic effects on innovative wind turbine concepts, in *High Performance Computing in Science and Engineering' 16* (Springer, Berlin, 2016), pp. 529–543
5. R. Gasch, J. Twele, *Windkraftanlagen: Grundlagen, Entwurf, Planung und Betrieb* (Springer, Berlin, 2010)
6. X. Huang, S. Vey, M. Meinke, W. Schroeder, G. Pechlivanoglou, C. Nayeri, C.O. Paschereit, Numerical and experimental investigation of wind turbine wakes, in *45th AIAA Fluid Dynamics Conference* (2015), p. 2310
7. A. Jameson, Time dependent calculations using multigrid, with applications to unsteady flows past airfoils and wings. AIAA Paper 1596:1991 (1991)
8. A. Jameson, W. Schmidt, E. Turkel et al., Numerical solutions of the euler equations by finite volume methods using Runge-Kutta time-stepping schemes. AIAA Paper 1259:1981 (1981)
9. E. Jost, A. Fischer, T. Lutz, E. Krämer, An investigation of unsteady 3d effects on trailing edge flaps. J. Phys.: Conf. Ser. **753**, 022009 (2016)
10. L. Klein, T. Lutz, E. Krämer, CFD analysis of a 2-bladed multi-megawatt turbine, in *10th PhD Seminar on Wind Energy in Europe*, EAWE, 2014, 28–31 October 2014, Orléans, pp. 47–50
11. L. Klein, C. Schulz, T. Lutz, E. Krämer et al., Influence of jet flow on the aerodynamics of a floating model wind turbine, in *The 26th International Ocean and Polar Engineering Conference* (International Society of Offshore and Polar Engineers, 2016)
12. U. Kowarsch, C. Öhrle, M. Keßler, E. Krämer, Aeroacoustic simulation of a complete h145 helicopter in descent flight. J. Am. Helicopter Soc. **61**(4), 1–13 (2016)
13. P.-Å. Krogstad, J. Lund, An experimental and numerical study of the performance of a model turbine. Wind Energy **15**(3), 443–457 (2012)
14. N. Kroll, C.-C. Rossow, K. Becker, F. Thiele, The megafLOW project. Aerosp. Sci. Technol. **4**(4), 223–237 (2000)
15. K. Meister, *Numerische Untersuchung zum aerodynamischen und aeroelastischen Verhalten einer Windenergieanlage bei turbulenter atmosphärischer Zuströmung* (Shaker Verlag, Herzogenrath, 2015)
16. C.N. Nayeri, S. Vey, D. Marten, G. Pechlivanoglou, C.O. Paschereit, X. Huang, M. Meinke, W. Schöder, G. Kampers, M. Hölling, J. Peinke, A. Fischer, T. Lutz, E. Krämer, U. Cordes, K. Hufnagel, K. Schiffmann, H. Spiegelberg, C. Tropea, Collaborative research on wind turbine load control under realistic turbulent inflow conditions, in *DEWEK* (2015)
17. G. Pechlivanoglou, J. Fischer, O. Eisele, S. Vey, C.N. Nayeri, C.O. Paschereit, Development of a medium scale research hawt for inflow and aerodynamic research in the TU Berlin wind tunnel. *DEWEK* (2015)
18. M. Sayed, T. Lutz, E. Krämer, Aerodynamic investigation of flow over a multi-megawatt slender bladed horizontal-axis wind turbine, in *Renewable Energies Offshore* (2015)
19. J. Schepers, H. Snel, Model experiments in controlled conditions. ECN Report (2007)
20. C. Schulz, L. Klein, P. Weihing, T. Lutz et al., CFD studies on wind turbines in complex terrain under atmospheric inflow conditions. J. Phys.: Conf. Ser. **524**, 012134 (2014)
21. C. Schulz, K. Meister, T. Lutz, E. Krämer, Investigations on the wake development of the Mexico rotor considering different inflow conditions, in *Contributions to the 19th STAB/DGLR Symposium Munich, Germany 2014*. Notes on Numerical Fluid Mechanics and Multidisciplinary Design. STAB (Springer, Berlin, 2014)
22. H. Schümann, F. Pierella, L. Sætran, Experimental investigation of wind turbine wakes in the wind tunnel. Energy Procedia **35**, 285–296 (2013)
23. N. Sorensen, J. Michelsen, S. Schreck, Navier-stokes predictions of the NREL phase vi rotor in the NASA ames 80-by-120 wind tunnel, in *ASME 2002 Wind Energy Symposium* (American Society of Mechanical Engineers, 2002), pp. 94–105
24. P. Weihing, K. Meister, C. Schulz, T. Lutz et al., CFD simulations on interference effects between offshore wind turbines. J. Phys.: Conf. Ser. **524**, 012143 (2014)